

# Isometric Energies for Recovering Injectivity in Constrained Mapping

Xingyi Du

Washington University in St. Louis  
USA  
du.xingyi@wustl.edu

Danny M. Kaufman

Qingnan Zhou  
Adobe Research  
USA  
kaufman@adobe.com  
qzhou@adobe.com

Shahar Z. Kovalsky

University of North Carolina at  
Chapel Hill (UNC)  
USA  
shaharkov@gmail.com

Yajie Yan

Independent researcher  
USA  
yajieyan@wustl.edu

Noam Aigerman

Adobe Research  
USA  
aigerman@adobe.com

Tao Ju

Washington University in St. Louis  
USA  
taoju@wustl.edu

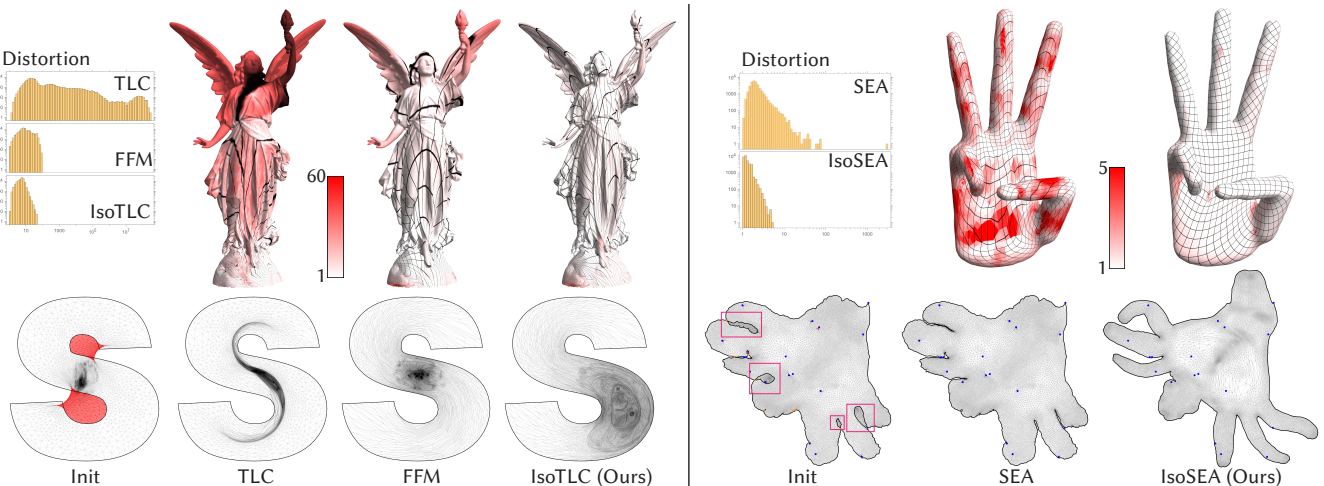


**Figure 1:** When used to parameterize meshes into the 2D plane, our isometric variants of injectivity energies empirically tend to yield injective results with low isometric distortion. Left: an initial map of Lucy into letter S, which contains many inverted triangles (red), is optimized while holding its boundary fixed, using the TLC energy [Du et al. 2020], the Fold-Free Mapping (FFM) method of [Garanzha et al. 2021], and our energy - IsoTLC. Right: an initial map, which contains inverted triangles (red), overwinding vertices (purple) and global overlaps (boxed), is optimized while fixing only a set of sparse positional constraints (blue) without constraining the boundary, by minimizing either the SEA energy of [Du et al. 2020] or our energy, IsoSEA. In both cases, our method leads to the injective map with the lowest isometric distortion ( $\max(\sigma_1, 1/\sigma_2)$ ) of the triangles, as shown by the histograms and the color map on the mesh.

## ABSTRACT

Computing injective maps with low distortions is a long-standing problem in computer graphics. Such maps are particularly challenging to obtain in the presence of positional constraints, because an injective initial map is often not available. Recently, several energies

were proposed and shown to be highly successful in optimizing injectivity from non-injective initial maps while satisfying positional constraints. However, minimizing these energies tends to produce elements with significant isometric distortions. This paper presents simple variants of these energies that retain their desirable traits while promoting isometry. While our method is not guaranteed to provide an injective map, we observe that, on large-scale 2D and 3D data sets, minimizing the proposed isometric variants results in a similar level of success in recovering injectivity as the original energies but a significantly lower isometric distortion.

## CCS CONCEPTS

- Computing methodologies → Mesh models.

Permission to make digital or hard copies of part or all of this work for personal or classroom use is granted without fee provided that copies are not made or distributed for profit or commercial advantage and that copies bear this notice and the full citation on the first page. Copyrights for third-party components of this work must be honored. For all other uses, contact the owner/author(s).

SA '22 Conference Papers, December 6–9, 2022, Daegu, Republic of Korea

© 2022 Copyright held by the owner/author(s).

ACM ISBN 978-1-4503-9470-3/22/12.

<https://doi.org/10.1145/3550469.3555419>

## KEYWORDS

Parameterization, mapping, injective

### ACM Reference Format:

Xingyi Du, Danny M. Kaufman, Qingnan Zhou, Shahar Z. Kovalsky, Yajie Yan, Noam Aigerman, and Tao Ju. 2022. Isometric Energies for Recovering Injectivity in Constrained Mapping. In *SIGGRAPH Asia 2022 Conference Papers (SA '22 Conference Papers)*, December 6–9, 2022, Daegu, Republic of Korea. ACM, New York, NY, USA, 9 pages. <https://doi.org/10.1145/3550469.3555419>

## 1 INTRODUCTION

This paper concerns recovering injective, low-distortion mappings of triangular and tetrahedral meshes under given constraints. The ability to compute such maps is crucial in a wide range of applications in computer graphics and geometry processing, such as texture mapping [Hormann et al. 2007], remeshing [Alliez et al. 2008], deformation [Zhu et al. 2018a], shape correspondence [Kraevoy and Sheffer 2004] and physical simulation [De Goes and James 2017].

Such tasks often involve three different requirements of the given map: 1) it usually needs to satisfy *positional constraints*, such as mapping a specific vertex of the mesh to a specific location. For instance, in texture mapping, a surface mesh may need to be mapped to a domain with a prescribed boundary, and additionally some internal vertices are required to align with corresponding locations in the texture image; 2) The map should have *low distortion*, preserving the shape of the original mesh as much as possible; 3) the map is one-to-one, i.e., *injective*, meaning that the mapped mesh does not have elements that overlap one another and each element has a positive area (or volume).

Unfortunately, satisfying all three properties simultaneously proves to be quite difficult: on one hand, there is no known method which is guaranteed to produce injective mappings for the given constraints. On the other hand, distortion optimization techniques usually require a *feasible initialization* (i.e., an initial map which is injective and satisfies the constraints). In some cases, even a feasible initial map may not be a good initializer for optimization methods, as high-distortion triangles lead to numerical issues which hinder convergence. In this paper, we tackle this problem and propose a method to compute injective, low-distortion, and constraint-satisfying maps, without assuming a proper initialization. This method can be used on its own in tasks which require such maps, or otherwise can be used in tandem with other map optimization techniques where our result can serve as a good initializer.

### 1.1 Review of injective and low-distortion mapping

Computing injective maps under positional constraints, let alone minimizing distortion, is a non-trivial task. In fact, it is only in the special case of mapping a triangular mesh to the 2D domain with a fixed convex boundary that an injective map can be directly obtained, via Tutte's embedding [Floater 2003; Tutte 1963]. This work has been extended to slightly-more complex domains [Aigerman and Lipman 2015]. However, no known method can guarantee injectivity for general types of positional constraints (e.g., non-convex boundaries or interior constraints), without altering the mesh structure, or for mapping 3D meshes.

A common paradigm is to minimize some distortion measure while *preserving* the injectivity of an initial map [Fu et al. 2015; Jiang et al. 2017; Levi and Zorin 2014; Liu et al. 2018, 2016; Myles and Zorin 2013; Rabinovich et al. 2017; Schüller et al. 2013; Smith and Schaefer 2015; Su et al. 2020], with efficient means developed to optimize these energies [Claici et al. 2017; Shtengel et al. 2017; Zhu et al. 2018b]. Such energies often act as a *barrier*, such as MIPS [Hormann and Greiner 2000] and Symmetric Dirichlet [Smith and Schaefer 2015], which is infinite on degenerate elements (with zero area of volume), thereby preventing elements from degeneration and inversion. However, these methods require an injective starting point, which is not available for general positional constraints. On the other hand, soft constraints with penalty energies can be added into these methods [Jiang et al. 2017], although constraint-satisfaction is not guaranteed.

An alternative approach is to *recover* injectivity from initial, non-injective maps while keeping the constraints fixed. Many such methods [Aigerman and Lipman 2013; Fu and Liu 2016; Hefetz et al. 2019; Kovalsky et al. 2015; Naitsat et al. 2020; Su et al. 2019; Xu et al. 2011] can produce low-distortion maps, but they often suffer from failure cases in which an injective map is not recovered.

Closer to our approach, a few recent methods show greater success in recovering injectivity by minimizing energies that are specifically designed to promote injectivity. Du et al. [2020] proposed to minimize the *Total Lifted Content* (TLC) energy to compute injective mapping with a fixed boundary. TLC is a smooth approximation of the total unsigned area (or volume) of the mapped elements. This energy was generalized to enable mapping triangular meshes to the plane with arbitrary positional constraints [Du et al. 2021]. The generalized energy, called *Smooth Excess Area* (SEA), is a smooth proxy of the total inverted and overlapping area. Both TLC and SEA are readily minimized by standard gradient-based solvers. However, a key limitation of both energies is that their minimization may result in significant isometric distortions (see Figure 1).

Recently, Garanzha et al. [2021] introduced a new energy for recovering inversion-free, constraint-satisfying maps that also have low isometric distortions. The authors apply the penalty technique of [Garanzha and Kaparin 1999] on a barrier energy to obtain a smooth function that heavily penalizes inverted elements while reducing both angle and area distortions of non-inverted elements. Using a customized solver, minimizing the energy yields maps with much lower distortions than [Du et al. 2020] while retaining its robustness in restoring injectivity (see Figure 1 left). However, the penalty energy does not consider overlaps between triangles, and hence it cannot be used as-is to recover injectivity when the boundary is not fully constrained.

Concurrent to our work, Wang et al. [Wang et al. 2022] presented a technique for free-boundary mapping of 2D meshes under positional constraints. Instead of proposing a new energy, the authors combine several existing methods (e.g., [Botsch and Kobelt 2004; Jiang et al. 2017; Su et al. 2019]) into a practically effective pipeline for achieving global injectivity with low distortions.

It is possible that an injective map satisfying the given positional constraints may not exist without altering the mesh connectivity (see Figure 3 in the Supplemental Materials). Methods that employ remeshing and refinement therefore have more flexibility in achieving injectivity [Agarwal et al. 2008; Campen et al. 2016; Gillespie

et al. 2021; Gu et al. 2018; Shen et al. 2019; Weber and Zorin 2014]. However, the resulting maps cannot be immediately utilized by applications that require adherence to the input mesh structure.

## 1.2 Contributions

As reviewed above, while the variational approach has been extensively used for recovering injectivity, energies that promote injective, low-distortion, and constraint-satisfying maps remain scarce. This paper makes another step towards filling this gap.

We propose a modification to the energies introduced in TLC [Du et al. 2020] and SEA [Du et al. 2021], which augments them from solely inducing injectivity to also reducing distortion. The modified energies, which we call *Isometric TLC* (IsoTLC) and *Isometric SEA* (IsoSEA), inherit the desirable traits of TLC and SEA: they are well-defined for both injective and non-injective maps, readily minimized (with a fixed parameter) using standard gradient-based solvers, and equipped with provable properties at global energy minima (even though such minima are unlikely to be reached in practice due to the non-convexity of the energies).

Our energies are evaluated on both fixed-boundary and free-boundary mapping benchmarks, and the resulting maps exhibit significantly lower isometric distortion than TLC and SEA (see Figure 1) while maintaining similarly high success rates in recovering injectivity. Furthermore, maps minimizing IsoTLC in the fixed-boundary benchmark typically have lower distortion than those produced by [Garanzha et al. 2021], most notably in 2D. Lastly, we show that our method can produce initial maps that facilitate distortion-optimization algorithms to achieve better convergence than starting from other initializers.

## 2 METHOD

### 2.1 Preliminaries

*Problem statement.* We assume to be given a *rest mesh*  $M$  whose elements are  $d$ -dimensional simplices (e.g., triangles, tetrahedra, etc.), embedded in  $\mathbb{R}^n$  for  $n \geq d$ . We assume that every element of  $M$  is *positively oriented* (i.e., having a positive  $d$ -dimensional volume) and no two elements overlap in their interior. The boundary of  $M$ ,  $\partial M$ , may consist of one or multiple connected components. Additionally, we are given a set of positional constraints, described as pairs of a vertex index and its desired target position in  $\mathbb{R}^d$ .

Our output is a piecewise-linear map  $T : M \rightarrow \mathbb{R}^d$ , i.e., a map which is linear over each element of  $M$ .  $T$  is represented via an assignment of new coordinates to each vertex of  $M$ , and we alternate between referring to  $T$  as both the map and the mapped mesh. We aim to output a map  $T$  that meets the following criteria, if it exists:

- (1) *Constraint-satisfying:* The positional constraints are all met.
- (2) *Globally injective (and non-inverting):* The mesh  $T$  has only positively oriented elements, and no two elements of  $T$  overlap in their interior.
- (3) *Low-distortion:* The map  $T$  should minimize both angle and area distortions.

Our approach modifies the injectivity-inducing energies TLC [Du et al. 2020] and SEA [Du et al. 2021] to also encourage low distortion. The core observation used in the derivation of both energies is that a piecewise-linear map  $T$  is injective if and only if all its

elements are positively oriented and the boundary map  $\partial T$  is injective [Lipman 2014]. Hence, these energies are formulated so as to ensure triangles have correct orientation. The boundary map can either be set to be injective via positional constraints, leading to the TLC energy, or otherwise be optimized along with the triangles' orientation, leading to the SEA energy.

*TLC for fixed-boundary mapping.* TLC assumes a given, fixed target boundary  $\partial T$ , possibly with additional interior constraints, and creates a smooth, robust proxy for the sum of unsigned volumes of all elements. The proxy is constructed by *lifting* the vertex coordinates of each  $d$ -dimensional simplex  $t$  of  $T$  to  $2d$  dimensions and measuring the volume of the lifted simplex. Specifically, lifting is controlled by two parameters, a positively oriented  $d$ -dimensional auxiliary simplex  $\tilde{t}$  and a non-negative scalar  $\alpha$ . Each vertex of the lifted simplex has coordinates  $\{x_1, \dots, x_d, \sqrt{\alpha}\tilde{x}_1, \dots, \sqrt{\alpha}\tilde{x}_d\}$ , where  $\{x_1, \dots, x_d\}$  are the coordinates of a vertex of  $t$  and  $\{\tilde{x}_1, \dots, \tilde{x}_d\}$  are the coordinates of the corresponding vertex of  $\tilde{t}$ . The volume of the lifted simplex is called the *lifted content* of  $t$  and denoted by  $A_{\tilde{t},\alpha}(t)$ . Du et al. [2020] show that, for any  $\alpha > 0$ ,  $A_{\tilde{t},\alpha}(t)$  is always positive and smooth, even if  $t$  is degenerate or inverted [Du et al. 2020]. The *Total Lifted Content* (TLC) of a mesh  $T$ , given a set of auxiliary simplices  $\tilde{T}$ , one for each element of  $T$ , is then defined as the sum,

$$A_{\tilde{T},\alpha}(T) = \sum_{t \in T} A_{\tilde{t},\alpha}(t) \quad (1)$$

Du et al. [2020] prove that, for  $d = 2, 3$  and assuming an injective map exists for the given boundary map, the minimizer of  $A_{\tilde{T},\alpha}(T)$  is injective for any choice of auxiliary simplices  $\tilde{T}$  and sufficiently small values of  $\alpha$ .

*SEA for free-boundary mapping.* SEA [Du et al. 2021] tackles cases where a triangular mesh ( $d = 2$ ) is to be mapped injectively but without necessarily constraining its boundary curve. They construct an energy that smoothly approximates the inverted and overlapping triangle areas. They define the *excess area* of  $T$  as

$$\sum_{t \in T} |A(t)| - O(\partial T), \quad (2)$$

where  $A(t)$  is the signed area of a triangle  $t$ , and  $O(C)$  is the *occupancy* of a closed curve  $C$  defined as the total area of the plane where the winding number is positive (the *winding number* of  $C$  around a point is the number of times that  $C$  travels around the point). The excess area is zero if and only if there is zero inverted or overlapping triangle area, which is equivalent to injectivity except for the presence of degenerate triangles.

A smooth proxy is devised by replacing the first term of the excess area with TLC and the second term with the *arc-occupancy*  $O_\theta(\partial T)$ , defined on a new curve that replaces each edge of  $\partial T$  with an arc of center angle  $\theta$ , leading to *Smooth Excess Area* (SEA),

$$A_{\tilde{T},\alpha,\theta}(T) = A_{\tilde{T},\alpha}(T) - O_\theta(\partial T). \quad (3)$$

Du et al. [2021] proved that, for sufficiently small  $\alpha$  and  $\theta$ , SEA is minimized by a locally injective map with bounded total overlapping area, where a map  $T$  is *locally injective* if it has only positively oriented elements and no two *vertex-adjacent* elements overlap.

We now begin deriving the modifications to the above energies in order to make them distortion-reducing.

## 2.2 Isometric TLC

*Distortion analysis.* We first analyze the relation between the TLC energy [Du et al. 2020] and the map's distortion when the boundary of the map is fully constrained. To do so, we introduce a singular-value form of the lifted content,  $A_{\tilde{t},\alpha}(t)$ . Denote  $L$  the matrix that transforms the edge vectors of  $\tilde{t}$  to the corresponding vectors of  $t$ , and  $\{\sigma_1, \dots, \sigma_d\}$  its singular values. Let  $A_{\tilde{t}}$  be the volume of the auxiliary simplex  $\tilde{t}$  (note that  $A_{\tilde{t}} > 0$ ). We show in the Supplemental Materials (Section 1) that,

$$A_{\tilde{t},\alpha}(t) = A_{\tilde{t}} \sqrt{\prod_{i=1}^d (\sigma_i^2 + \alpha)}. \quad (4)$$

It is helpful to examine the *residue* of the lifted content of  $t$  after subtracting its signed volume,

$$\begin{aligned} R(t) &= A_{\tilde{t},\alpha}(t) - A(t) \\ &= A_{\tilde{t}} \left( \sqrt{\prod_{i=1}^d (\sigma_i^2 + \alpha)} - \det(L) \right). \end{aligned} \quad (5)$$

Since the lifted content  $A_{\tilde{t},\alpha}(t)$  approximates the unsigned volume  $|A(t)|$ , the residue  $R(t)$  approximates the *inverted volume* of  $t$ . Note that  $R(t)$  is a smooth function in  $t$ , and its sum over all elements of  $T$  differs from TLC only by the total signed volumes, which is a constant if the boundary is fully constrained. As a result, the sum of  $R(t)$  over all elements shares the same energy minimizer as TLC.

We next show that  $R(t)$  is minimized by a *similarity* transformation in two dimensions and by a singular map in higher dimensions (see proof in Supplemental Materials, Section 2):

**PROPOSITION 2.1.** *For any  $\alpha > 0$ ,  $R(t) \geq \alpha^{\frac{d}{2}} A_{\tilde{t}}$ . Equality holds when either of the following holds:*

- (1)  $d = 2$ ,  $\sigma_1 = \sigma_2$  and  $\det(L) \geq 0$ .
- (2)  $d > 2$  and  $\sigma_1 = \dots = \sigma_d = 0$ .

We visualize the residue  $R(t)$  for  $d = 2$  in Figure 2 (a) as a function of  $\sigma_1, \sigma_2$  ( $\sigma_1$  is given the sign of  $\det(L)$ ). Observe that the function is smoothly defined even when  $t$  is inverted ( $\det(L) < 0$ ) or degenerate ( $|\det(L)| = \sigma_1 \sigma_2 = 0$ ), and it reaches its minimum when  $\sigma_1 = \sigma_2$ . Note that such minimizers are scale-invariant, which explains the extremely small triangles after minimizing TLC (see Figure 1 left).

*Energy modification.* To reduce the area distortions created when minimizing TLC, we introduce another smooth measure that approximates the unsigned volume  $|A(t)|$ . Unlike the lifted content, the residue of this measure after subtracting  $A(t)$  is minimized by an *isometry*. The measure, which we call the *isometric lifted content*, has the form:

$$A_{\tilde{t},\alpha}^{iso}(t) = \sqrt{A(t)^2 + \frac{\alpha}{2^{d-1}} A_{\tilde{t},1}(t)^2 + \alpha^2 A_{\tilde{t}}^2}. \quad (6)$$

Inside the square root is a weighted sum of squares of the volume of the simplex ( $A(t)$ ), the lifted content at unit scale ( $A_{\tilde{t},1}(t)$ ), and the volume of the auxiliary simplex ( $A_{\tilde{t}}$ ). Using the singular-value form of the lifted content (Equation 4), we obtain an alternative form of isometric lifted content,

$$A_{\tilde{t},\alpha}^{iso}(t) = A_{\tilde{t}} \sqrt{\prod_{i=1}^d \sigma_i^2 + \frac{\alpha}{2^{d-1}} \prod_{i=1}^d (\sigma_i^2 + 1) + \alpha^2}. \quad (7)$$

It is easy to see that, like the lifted content, the isometric lifted content is smoothly defined over  $t$  and greater than  $|A(t)|$  for any  $\alpha > 0$ . We now analyze its residue after subtracting  $A(t)$ ,

$$\begin{aligned} R^{iso}(t) &= A_{\tilde{t},\alpha}^{iso}(t) - A(t) \\ &= A_{\tilde{t}} \left( \sqrt{\prod_{i=1}^d \sigma_i^2 + \frac{\alpha}{2^{d-1}} \prod_{i=1}^d (\sigma_i^2 + 1) + \alpha^2} - \det(L) \right). \end{aligned} \quad (8)$$

As shown below,  $R^{iso}(t)$  is minimized in any dimension  $d$  only when  $t, \tilde{t}$  are congruent (see proof in Supplemental Materials, Section 2):

**PROPOSITION 2.2.** *For any  $\alpha > 0$ ,  $R^{iso}(t) \geq \alpha A_{\tilde{t}}$ , and equality holds only when  $\sigma_1 = \dots = \sigma_d = 1$  and  $\det(L) > 0$ .*

We visualize  $R^{iso}(t)$  for  $d = 2$  in Figure 2 (b,c) for two different  $\alpha$  values (0.1,1). Observe that  $R^{iso}(t)$ , like  $R(t)$ , is smooth for all  $t$ , but it reaches minimum at  $\sigma_1 = \sigma_2 = 1$ . We further compare with the penalty energy of [Garanzha et al. 2021] defined over a single triangle. This energy is a weighted sum of angle and area distortion measures (we set weight  $\lambda = 1$  as suggested in the paper), and it is controlled by a parameter  $\epsilon$ . As  $\epsilon$  decreases, the energy approaches a barrier function that is infinite when the triangle is degenerate or inverted. We visualize their energy in Figure 2 (d,e,f) for three different values of  $\epsilon = 0.1, 0.5, 1$ . Observe that the penalty energy is smoothly defined and penalizes triangle inversion. However, its energy minimum drifts away from isometry ( $\sigma_1 = \sigma_2 = 1$ ) towards the singular map ( $\sigma_1 = \sigma_2 = 0$ ) as  $\epsilon$  increases. In contrast, the minimum of  $R^{iso}(t)$  stays at isometry regardless of  $\alpha$ .

We define the *Isometric TLC* (IsoTLC) of a mesh  $T$  as the sum of isometric lifted content of all elements of  $T$ ,

$$A_{T,\alpha}^{iso}(T) = \sum_{t \in T} A_{\tilde{t},\alpha}^{iso}(t) \quad (9)$$

A key property of TLC for  $d = 2, 3$ , as mentioned earlier, is the injectivity of maps attaining the global minimum, if the problem is feasible (again, we note that reaching the global minimum in practice is unlikely due to the nonconvexity of the energy). IsoTLC shares the same property for any  $d \geq 2$  (see Supplemental Materials, Section 3):

**PROPOSITION 2.3.** *Let  $T_0$  be an injective map with a fully constrained boundary and possible interior constraints. Then there exists some  $\alpha_0 > 0$  such that  $A_{T,\alpha}^{iso}(T) > A_{T,\alpha}^{iso}(T_0)$  for any  $\alpha < \alpha_0$  and any non-injective map  $T$  satisfying the same constraints.*

We compare the results of minimizing TLC and IsoTLC in Figure 3. The rest mesh  $M$  is used as the auxiliary elements  $\tilde{T}$  for both energies. Observe that minimizing IsoTLC at different  $\alpha$  results in injective maps with similar appearances, all with much lower distortions than maps minimizing TLC.

## 2.3 Isometric SEA

*Distortion analysis.* To see how the SEA energy [Du et al. 2021] is related to map distortion, consider a map  $T$  with a non-intersecting boundary  $\partial T$ . According to Lemma C.1 in [Du et al. 2021], the arc-occupancy  $O_\theta(\partial T)$  reduces to the occupancy  $O(\partial T)$  for any  $\theta < \theta_0$  where  $\theta_0$  is a positive constant determined by  $\partial T$ . Since  $\partial T$  is non-intersecting,  $O(\partial T)$  is simply the area bounded by the curve,

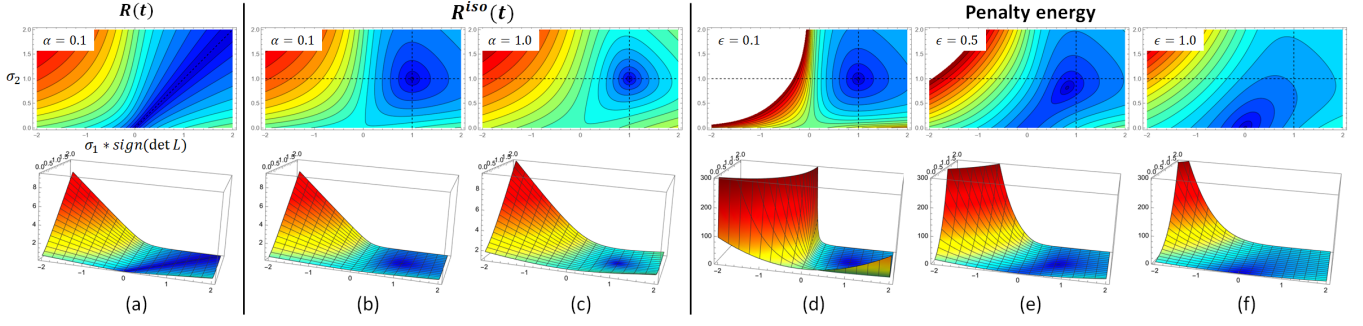


**Figure 2: Visualizing  $R(t)$  (a),  $R^{iso}(t)$  at different  $\alpha$  values (b,c), and the penalty energy of [Garanzha et al. 2021] at different  $\epsilon$  (d,e,f) as functions of the singular values  $\sigma_1, \sigma_2$  of the linear transform  $L$  from  $\tilde{t}$  to  $t$  ( $\sigma_1$  is given the sign of  $\det(L)$ ). Observe that  $R(t)$  is minimized by a similarity transform ( $\sigma_1 = \sigma_2$ ),  $R^{iso}(t)$  is minimized by an isometry ( $\sigma_1 = \sigma_2 = 1$ ) regardless of  $\alpha$ , and the minimizer of the penalty energy drifts away from isometry as  $\epsilon$  increases.**

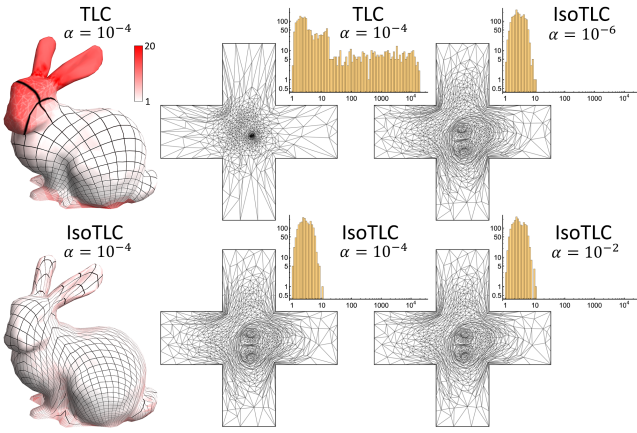


**Figure 3: Optimizing an initial map of the Bunny mesh into a non-convex boundary by minimizing (till convergence) the TLC energy and our IsoTLC variant (at different  $\alpha$ ). The histograms show the triangle distortions using the measure  $\max(\sigma_1, 1/\sigma_2)$  (assuming  $\sigma_1 \geq \sigma_2$ ).**

which equals the sum of signed triangle areas of  $T$ . So, for such a pair  $\{T, \theta\}$ , SEA reduces to a measure of the inverted triangle areas,

$$A_{\tilde{T}, \alpha, \theta}(T) = A_{\tilde{T}, \alpha}(T) - \sum_{t \in T} A(t) = \sum_{t \in T} R(t). \quad (10)$$

Here  $R(t)$  is the residue defined in Equation 5, which is minimized by a similarity transformation from the auxiliary simplex  $\tilde{T}$ . As a result, minimizing SEA on a mesh with an intersection-free boundary tends to suppress angle distortion from the auxiliary simplices  $\tilde{T}$ , but at the cost of possibly significant area distortions (see Figure 1 right).

*Energy modification.* To penalize isometric distortions, we modify SEA by replacing the TLC term with the proposed IsoTLC,

$$A_{\tilde{T}, \alpha, \theta}^{iso}(T) = A_{\tilde{T}, \alpha}^{iso}(T) - O_\theta(\partial T). \quad (11)$$

We call this variant the *Isometric SEA* (IsoSEA). Following the reasoning above, for any map  $T$  with a non-intersecting boundary

and some range of small  $\theta$ , IsoSEA reduces to the sum of residues  $R^{iso}(t)$  over all elements  $t \in T$ . Since  $R^{iso}(t)$  is minimized by an isometry from  $\tilde{T}$ , minimizing IsoSEA has the effect of reducing both angle and area distortions from  $\tilde{T}$ .

IsoSEA preserves the key properties of SEA. Since IsoTLC, like TLC, is smooth over the space of all maps, IsoSEA maintains the smoothness of SEA. Furthermore, we can show that IsoSEA inherits the same theoretical property as SEA: assuming an injective constraint-satisfying map exists, and for sufficiently small  $\alpha$  and  $\theta$ , IsoSEA is minimized only by a locally injective map with a bounded total overlapping area. The property is formally stated as follows (see proof in Supplemental Materials, Section 4):

**PROPOSITION 2.4.** *Let  $T_0$  be an injective, triangular map satisfying the given constraints. For any  $\lambda > 0$ , there exists some  $\alpha_0 > 0$  and  $\theta_0 > 0$  such that, for any  $\alpha < \alpha_0, \theta < \theta_0$ ,  $A_{\tilde{T}, \alpha, \theta}^{iso}(T) > A_{\tilde{T}, \alpha, \theta}^{iso}(T_0)$  for any map  $T$  that is not locally injective or whose overlapping area is greater than  $\lambda$ .*

## 2.4 Optimization

Our variants of TLC and SEA, like the original energies, can be readily minimized using standard gradient-based methods. We implemented a quasi-Newton (QN) method using an off-the-shelf BFGS solver [Wright and Nocedal 1999] for both IsoTLC and IsoSEA. Since IsoTLC has higher-order smoothness, we adopted the projected-Newton (PN) method in [Du et al. 2020] that ensures positive-definiteness of the global Hessian matrix by projecting per-simplex Hessians. We derived analytical expressions for the gradient and (projected) Hessian of IsoTLC from the singular-value form of the isometric lifted content (Equation 7) using the technique of [Smith et al. 2019] (see Supplemental Materials, Section 5, for details).

Despite our theoretical analysis of map injectivity at the minima of IsoTLC and IsoSEA, gradient-based solvers have no guarantee of reaching the global minimum of these non-convex energies. In practice, we adopt a two-step approach that first attempts to find an injective map and, if successful, then lowers its distortion:

- (1) Computing injective maps: Following the same strategy in [Du et al. 2020, 2021], we first run QN until an injective map is found, or the energy has converged, or a maximum  $N$

iterations is reached (we use  $N = 10000$ ). If IsoTLC is being minimized and an injective map is not found, we repeat the same process with PN from the initial map.

- (2) Lowering distortion: If the previous step produces an injective map, we then run PN (for IsoTLC) or QN (for IsoSEA) to continue minimizing the energy for another  $N$  iterations or until the energy converges. If the resulting map is non-injective, we output the last injective map obtained during the iterations.

### 3 RESULTS

We evaluate our IsoTLC and IsoSEA energies on existing benchmarks for both fixed-boundary and free-boundary mapping, and we compare the injectivity and distortion of the resulting maps with existing methods. We implemented the optimization strategy in Section 2.4 in C++. Eigen was used for matrix operations. Evaluating the arc-occupancy term in SEA and IsoSEA requires computing the pairwise intersection of circular arcs. We follow [Du et al. 2021] and used OpenMP to parallelize this step. More implementation details are provided in Supplemental Materials (Section 5).

The only parameters in our method are scalars  $\alpha, \theta$ . We observed that while a larger  $\alpha$  generally leads to smoother energy landscapes and faster convergence, optimizing with a smaller  $\alpha$  is more likely to reach an injective map (which is consistent with Propositions 2.3,2.4). We found that setting  $\alpha = 10^{-4}$  in both IsoTLC and IsoSEA and  $\theta = 0.1$  in IsoSEA maximizes the success rate in recovering injectivity within the allowed number of iterations.

We use the rest meshes  $M$  provided in the benchmark as the auxiliary simplices  $\tilde{T}$ , which enables both IsoTLC and IsoSEA to reduce isometric distortions from  $M$ . In contrast, equilateral triangles (and tetrahedra) were used as auxiliary simplices for minimizing TLC and SEA in [Du et al. 2020, 2021]. The choice was made to boost the success rate in recovering injectivity, as these energies are not concerned with map distortion.

To measure isometric distortion, we consider  $\max(\sigma_1, 1/\sigma_2)$  in 2D and  $\max(\sigma_1, 1/\sigma_3)$  in 3D. This measure reaches the minimum of 1 only when  $t$  is congruent with  $\tilde{t}$ . We define the *maximum* and *average* distortion of a map as the maximum and mean per-element distortion over all elements.

#### 3.1 Fixed-boundary mapping benchmark

We first evaluated the IsoTLC energy on the benchmark data set in [Du et al. 2020], which consists of more than 10,000 2D examples and more than 900 3D examples of fixed-boundary mapping. Most examples were taken from real-world parameterization and deformation problems, but some of them are hand-crafted stress tests such as mapping a complex mesh into the outline of a letter (e.g., Figure 1 left). Each example comes with a rest mesh and an initial non-injective map into a fixed boundary, and all examples are known to have feasible (injective) solutions.

Our method achieved 100% success rate in recovering injectivity on this benchmark. To the best of our knowledge, only the original TLC method [Du et al. 2020] and the method of [Garanzha et al. 2021] (which we call FFM) have passed this benchmark with complete success. Furthermore, the maps produced by minimizing IsoTLC exhibit much lower isometric distortion than both of these

methods. As seen in the histograms Figure 4 (a,b), both the maximum and average distortion of 2D maps minimizing IsoTLC are a few orders of magnitude lower than those minimizing TLC or produced by FFM. Similarly observations can be made for 3D maps, except in the case of average distortion where IsoTLC and FFM are similar.

Figure 1 left shows one example from the 2D benchmark and compares the results of the three methods. Observe from the histograms that the TLC-minimizing map contains many elements with high distortion – up to seven orders of magnitude higher than elements in the IsoTLC-minimizing map or that produced by FFM. On the other hand, minimizing IsoTLC produces more elements with lower distortion than FFM. We provide more visual comparisons in Supplemental Materials (Section 6.1).

#### 3.2 Free-boundary mapping benchmark

We next evaluate the IsoSEA energy on the benchmark data set of [Du et al. 2021], which consists of nearly 1800 examples of mapping triangular meshes onto the plane with arbitrary positional constraints. Each example comes with a rest mesh (a triangular mesh in 3D), a constraint set of up to 20 vertices and their designated locations in the plane, and an initial map that satisfies those constraints but contains inverted or overlapping triangles. As in the fixed-boundary benchmark, each example in this benchmark has a feasible (injective and constraint-satisfying) solution.

Our method successfully recovered injectivity for 82% of examples in this challenging benchmark. This rate is slightly lower than the original SEA method [Du et al. 2021], which was successful on 85% of examples. Figure 5 examines two examples, one on which SEA succeeded but IsoSEA failed, and one on which IsoSEA succeeded but SEA failed. In the former case, the IsoSEA failure was caused by two parts of the mesh deeply crossing each other, which is a typical situation of slow convergence for both IsoSEA and SEA (see an illustrative example in Figure 15 of [Du et al. 2021]). In the latter case, the SEA failure was caused by several extremely small inverted triangles, a consequence of high isometric distortions. In contrast, by promoting isometry, IsoSEA successfully resolved all inverted triangles in this region in the initial map. Note that both methods were significantly more successful than previous methods designed to suppress only inverted triangles, such as [Fu and Liu 2016] and [Kovalsky et al. 2015], which recovered injectivity for less than 4% of examples in this benchmark as reported in [Du et al. 2021].

For those benchmark examples where both SEA and IsoSEA successfully produced injective maps, maps minimizing our IsoSEA energy exhibited significantly reduced isometric distortion than those minimizing SEA, as shown in the histograms of Figure 4 (c). Figure 1 right visually compares the results of the two methods on one example from the benchmark. Observe from the histograms that the SEA-minimizing map contains elements with up to two orders of magnitude higher distortion than elements in the IsoSEA-minimizing map. We provide more visual comparisons in Supplemental Materials (Section 6.1).

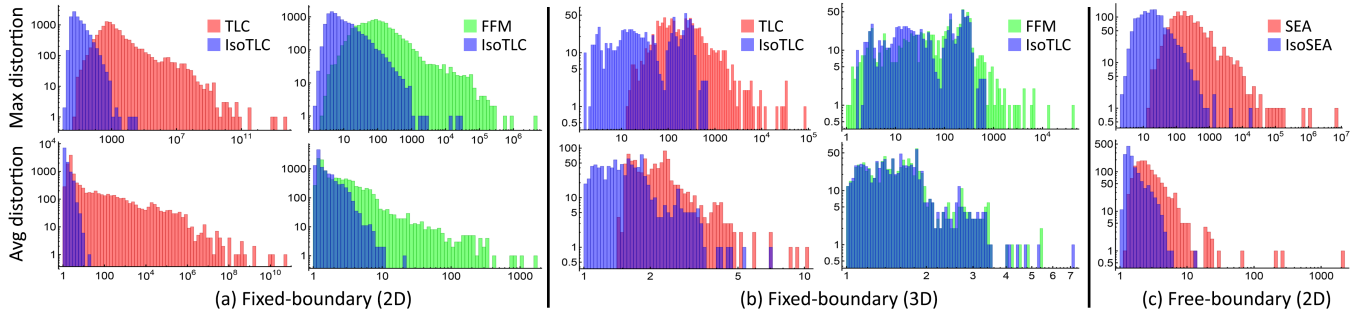


**Figure 4: Histograms (in log-log scale) of maximum (top) and average (bottom) distortion of maps computed by different methods on the fixed-boundary 2D (a) and 3D (b) benchmarks and the free-boundary benchmark (c) (only including examples where both SEA and IsoSEA succeeded in recovering injectivity).**

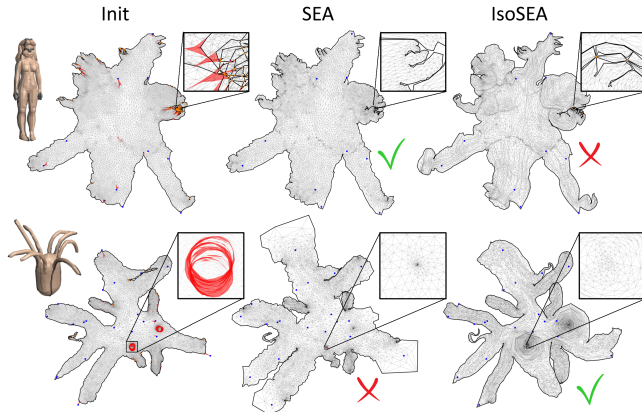


**Figure 5: Examples from the fixed-boundary benchmark where SEA succeeded in recovering injectivity from the initial map but IsoSEA failed (top) or vice versa (bottom). Top inserts: a region where IsoSEA produces boundary intersections (orange). Bottom inserts: a region where SEA results in inverted triangles (red).**

### 3.3 Performance

We report the running time of our algorithm on the fixed-boundary and free-boundary benchmarks as a function of mesh size in Figure 6. The timing was recorded on a Intel Core i9 CPU at 3.7GHz with 64 GB memory. We also separately report the timing for the first stage of our algorithm (computing an injective mesh).

Observe that the complexity of our algorithm generally grows with the mesh size. IsoSEA takes much longer to minimize than IsoTLC, as it needs to compute the arrangement of the boundary curve for the arc-occupancy term. These timings are similar to those of minimizing TLC and SEA as reported in [Du et al. 2020, 2021] and are comparable to those of [Garanzha et al. 2021] on the fixed-boundary benchmark. Finally, note that the second stage of our algorithm (lowering distortion of an already injective map) usually takes much longer than the first stage, since it only terminates at energy convergence or the maximum number of iterations.

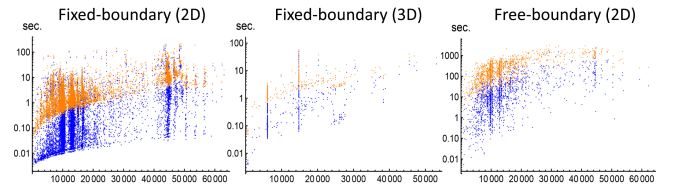


**Figure 6: Running time (seconds in log scale) versus mesh size (number of vertices) for all examples in the fixed-boundary 2D and 3D benchmarks and the free-boundary benchmark. Orange dots are times of the entire algorithm while blue dots are times of the first stage (computing injective maps).**

### 3.4 Initializing map optimization

With the ability to produce injective maps satisfying positional constraints, our method as well as [Du et al. 2020, 2021; Garanzha et al. 2021] can serve as the starting point for many existing constrained map optimization methods that require an injective initial mesh. Most of these optimization methods require computing the gradient or Hessians of some non-linear energy. Such computation may encounter numerical issues if the elements are too small, which in turn leads to slow or stalled convergence. As a result, the lower isometric distortions offered by our method can improve the convergence of these optimization methods.

As an example, we compare TLC and IsoTLC as initializers for fixed-boundary map optimization in Figure 7. Minimization TLC from an initially non-injective map (from Lucy to letter G) recovers an injective mesh with many extremely small triangles (as seen in the histogram of per-element distortion). Further optimizing this map by minimizing the Symmetric Dirichlet energy [Smith and Schaefer 2015] using a standard method [Zhu et al. 2018b], while keeping the boundary fixed, terminates after just a few iterations due to divergent energy and fails to improve upon the TLC result. Similar failures were observed on 6 out of the 30 examples from the benchmark of [Du et al. 2020] that map 3D surfaces to letter-like 2D domains. In contrast, IsoTLC minimization yields an injective map with much lower distortions, and further optimization of the Symmetric Dirichlet energy was able to converge with an even lower isometric distortion.

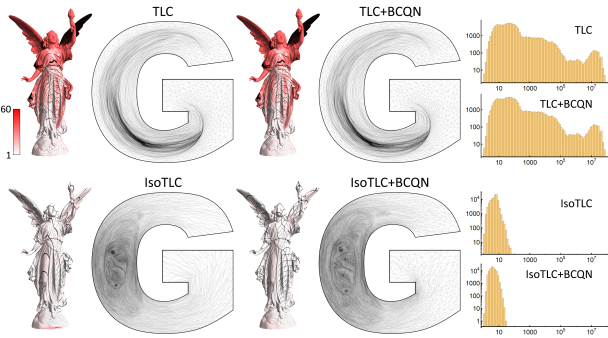


**Figure 7: Comparing maps produced by minimizing TLC and IsoTLC (mapping Lucy to letter G) as initialization for constrained optimization in BCQN [Zhu et al. 2018b] that minimizes the Symmetric Dirichlet energy. With the TLC map as the starting point, BCQN terminates in 4 iterations and the map remains highly distorted.**

## 4 DISCUSSION

While we have improved the distortion aspect of existing energies, TLC [Du et al. 2020] and SEA [Du et al. 2021], our energies retain some of their limitations. First, the rate of convergence of our energies may be strongly affected by the choice of the initial map, and our method may fail to produce injective maps within the allotted number of iterations for pathological initializations (see the TLC failure in Figure 5 of [Garanzha et al. 2021] and SEA failure in Figure 16 of [Du et al. 2021]; more IsoTLC failure examples are provided in Supplemental Materials, Section 6.2). Second, like SEA, our IsoSEA energy exhibits slow convergence when mesh parts deeply cross each other (Figure 5), which accounts for majority of our failure cases in the free-boundary benchmark. Third, our methods cannot produce injective maps for problems that do not have a feasible solution (see examples in Supplemental Materials, Section 6.2). Some potential directions for improving the convergence rate include adapting the parameters  $\alpha, \theta$  to either the mesh elements or the stage of optimization (as done in [Garanzha et al. 2021]) and designing higher-order variants of the arc-occupancy term in IsoSEA.

## ACKNOWLEDGMENTS

This work is supported in part by a gift from Adobe Research. We would like to thank authors of several papers for providing code, data, and help with our experiments.

## REFERENCES

- Pankaj K Agarwal, Bardia Sadri, and Hai Yu. 2008. Untangling triangulations through local explorations. In *Proceedings of the twenty-fourth annual symposium on Computational geometry*. ACM, 288–297.
- Noam Aigerman and Yaron Lipman. 2013. Injective and bounded distortion mappings in 3D. *ACM Transactions on Graphics (TOG)* 32, 4 (2013), 106.
- Noam Aigerman and Yaron Lipman. 2015. Orbifold Tutte embeddings. *ACM Trans. Graph.* 34, 6 (2015), 190–1.
- Pierre Alliez, Giuliana Ucelli, Craig Gotsman, and Marco Attene. 2008. Recent advances in remeshing of surfaces. *Shape analysis and structuring* (2008), 53–82.
- Mario Botsch and Leif Kobbelt. 2004. A remeshing approach to multiresolution modeling. In *Proceedings of the 2004 Eurographics/ACM SIGGRAPH symposium on Geometry processing*. 185–192.
- Marcel Campen, Cláudio T Silva, and Denis Zorin. 2016. Bijective maps from simplicial foliations. *ACM Transactions on Graphics (TOG)* 35, 4 (2016), 74.
- Sebastian Claici, Mikhail Bessmel'tsev, Scott Schaefer, and Justin Solomon. 2017. Isometry-Aware Preconditioning for Mesh Parameterization. In *Computer Graphics Forum*, Vol. 36. Wiley Online Library, 37–47.
- Fernando De Goes and Doug L James. 2017. Regularized kelvinlets: sculpting brushes based on fundamental solutions of elasticity. *ACM Transactions on Graphics (TOG)* 36, 4 (2017), 1–11.
- Xingyi Du, Noam Aigerman, Qingnan Zhou, Shahar Z Kovalsky, Yajie Yan, Danny M Kaufman, and Tao Ju. 2020. Lifting simplices to find injectivity. *ACM Transactions on Graphics (TOG)* 39, 4 (2020), 120–1.
- Xingyi Du, Danny M Kaufman, Qingnan Zhou, Shahar Z Kovalsky, Yajie Yan, Noam Aigerman, and Tao Ju. 2021. Optimizing global injectivity for constrained parameterization. *ACM Transactions on Graphics (TOG)* 40, 6 (2021), 1–18.
- Michael Floater. 2003. One-to-one piecewise linear mappings over triangulations. *Math. Comp.* 72, 242 (2003), 685–696.
- Xiao-Ming Fu and Yang Liu. 2016. Computing inversion-free mappings by simplex assembly. *ACM Transactions on Graphics (TOG)* 35, 6 (2016), 216.
- Xiao-Ming Fu, Yang Liu, and Baining Guo. 2015. Computing locally injective mappings by advanced MIPS. *ACM Transactions on Graphics (TOG)* 34, 4 (2015), 71.
- VA Garanzha and IE Kaparin. 1999. Regularization of the barrier variational method. *Computational mathematics and mathematical physics* 39, 9 (1999), 1426–1440.
- Vladimir Garanzha, Igor Kaparin, Liudmila Kudryavtseva, François Protais, Nicolas Ray, and Dmitry Sokolov. 2021. Foldover-free maps in 50 lines of code. *ACM Transactions on Graphics (TOG)* 40, 4 (2021), 1–16.
- Mark Gillespie, Boris Springborn, and Keenan Crane. 2021. Discrete conformal equivalence of polyhedral surfaces. *ACM Transactions on Graphics (TOG)* 40, 4 (2021), 1–20.
- Xianfeng Gu, Ren Guo, Feng Luo, Jian Sun, Tianqi Wu, et al. 2018. A discrete uniformization theorem for polyhedral surfaces II. *Journal of differential geometry* 109, 3 (2018), 431–466.
- Eden Fedida Hefetz, Edward Chien, and Ofir Weber. 2019. A Subspace Method for Fast Locally Injective Harmonic Mapping. In *Computer Graphics Forum*, Vol. 38. Wiley Online Library, 105–119.
- Kai Hormann and Giintner Greiner. 2000. MIPS: An Efficient Global Parametrization Method. *France on 1–7 July 1999. Proceedings, Volume 1. Curve and Surface Design. F61775–99-WF068* (2000), 153.
- Kai Hormann, Bruno Lévy, and Alla Sheffer. 2007. Mesh parameterization: Theory and practice. (2007).
- Zhongshi Jiang, Scott Schaefer, and Daniele Panozzo. 2017. Simplicial complex augmentation framework for bijective maps. *ACM Transactions on Graphics* 36, 6 (2017).
- Shahar Z Kovalsky, Noam Aigerman, Ronen Basri, and Yaron Lipman. 2015. Large-scale bounded distortion mappings. *ACM Trans. Graph.* 34, 6 (2015), 191–1.
- Vladislav Kraevoy and Alla Sheffer. 2004. Cross-parameterization and compatible remeshing of 3D models. *ACM Transactions on Graphics (TOG)* 23, 3 (2004), 861–869.
- Zohar Levi and Denis Zorin. 2014. Strict minimizers for geometric optimization. *ACM Transactions on Graphics (TOG)* 33, 6 (2014), 1–14.
- Yaron Lipman. 2014. Bijective Mappings of Meshes with Boundary and the Degree in Mesh Processing. *SIAM Journal on Imaging Sciences [electronic only]* 7 (04 2014). <https://doi.org/10.1137/130939754>
- Ligang Liu, Chunyang Ye, Ruiqi Ni, and Xiao-Ming Fu. 2018. Progressive parameterizations. *ACM Transactions on Graphics (TOG)* 37, 4 (2018), 41.
- Tiantian Liu, Ming Gao, Lifeng Zhu, Eftychios Sifakis, and Ladislav Kavan. 2016. Fast and Robust Inversion-Free Shape Manipulation. In *Computer Graphics Forum*, Vol. 35. Wiley Online Library, 1–11.
- Ashish Myles and Denis Zorin. 2013. Controlled-distortion constrained global parametrization. *ACM Transactions on Graphics (TOG)* 32, 4 (2013), 1–14.
- Alexander Naitsat, Yufeng Zhu, and Yehoshua Zeevi. 2020. Adaptive Block Coordinate Descent for Distortion Optimization. *Computer Graphics Forum* 39 (06 2020). <https://doi.org/10.1111/cgf.14043>
- Michael Rabinovich, Roi Poranne, Daniele Panozzo, and Olga Sorkine-Hornung. 2017. Scalable locally injective mappings. *ACM Transactions on Graphics (TOG)* 36, 4 (2017), 37a.
- Christian Schüller, Ladislav Kavan, Daniele Panozzo, and Olga Sorkine-Hornung. 2013. Locally injective mappings. In *Proceedings of the Eleventh Eurographics/ACMSIGGRAPH Symposium on Geometry Processing*. Eurographics Association, 125–135.
- Hanxiao Shen, Zhongshi Jiang, Denis Zorin, and Daniele Panozzo. 2019. Progressive embedding. *ACM Transactions on Graphics (TOG)* 38, 4 (2019), 32.
- Anna Shtengel, Roi Poranne, Olga Sorkine-Hornung, Shahar Z Kovalsky, and Yaron Lipman. 2017. Geometric optimization via composite majorization. *ACM Trans. Graph.* 36, 4 (2017), 38–1.
- Breannan Smith, Fernando De Goes, and Theodore Kim. 2019. Analytic eigensystems for isotropic distortion energies. *ACM Transactions on Graphics (TOG)* 38, 1 (2019), 1–15.

- Jason Smith and Scott Schaefer. 2015. Bijective parameterization with free boundaries. *ACM Transactions on Graphics (TOG)* 34, 4 (2015), 70.
- Jian-Ping Su, Xiao-Ming Fu, and Ligang Liu. 2019. Practical Foldover-Free Volumetric Mapping Construction. In *Computer Graphics Forum*, Vol. 38. Wiley Online Library, 287–297.
- Jian-Ping Su, Chunyang Ye, Ligang Liu, and Xiao-Ming Fu. 2020. Efficient bijective parameterizations. *ACM Transactions on Graphics (TOG)* 39, 4 (2020), 111–1.
- William Thomas Tutte. 1963. How to draw a graph. *Proceedings of the London Mathematical Society* 3, 1 (1963), 743–767.
- Qi Wang, Wen-Xiang Zhang, Yuan-Yuan Cheng, Ligang Liu, and Xiao-Ming Fu. 2022. Practical Construction of Globally Injective Parameterizations with Positional Constraints. *Computational Visual Media* (2022).
- Ofir Weber and Denis Zorin. 2014. Locally injective parametrization with arbitrary fixed boundaries. *ACM Transactions on Graphics (TOG)* 33, 4 (2014), 75.
- Stephen J Wright and Jorge Nocedal. 1999. *Numerical optimization*. Vol. 2. Springer New York.
- Yin Xu, Renjie Chen, Craig Gotsman, and Ligang Liu. 2011. Embedding a triangular graph within a given boundary. *Computer Aided Geometric Design* 28, 6 (2011), 349–356.
- Yufeng Zhu, Robert Bridson, and Danny M. Kaufman. 2018a. Blended Cured Quasi-Newton for Distortion Optimization. *ACM Trans. on Graphics (SIGGRAPH 2018)* (2018).
- Yufeng Zhu, Robert Bridson, and Danny M Kaufman. 2018b. Blended cured quasi-newton for distortion optimization. *ACM Transactions on Graphics (TOG)* 37, 4 (2018), 40.